frontiers | Frontiers in Analytical Science

TYPE Original Research
PUBLISHED 19 February 2025
DOI 10.3389/frans.2025.1533486

OPEN ACCESS

EDITED BY
Marianne Fillet,
University of Liège, Belgium

REVIEWED BY
Qingchun Lan,
Fudan University, China
Kumar Katragunta,
University of Mississippi, United States

*CORRESPONDENCE
Jianping Chen,
lycjp@126.com
Jihang Chen,
chenjihang@cuhk.edu.cn

†These authors have contributed equally to this work

RECEIVED 24 November 2024
ACCEPTED 10 January 2025
PUBLISHED 19 February 2025

CITATION
Cheng J, Meng X, Fang D, Zhu Y, Liu Z, Li X, Jie K, Huang S, Li H, Zhang S, Chen J and Chen J (2025) The chemicalome profiling of Zishen Yuzhen Pill *in vivo* and its promoting effect on osteogenic differentiation of MC3T3-E1 cells. *Front. Anal. Sci.* 5:1533486.
doi: 10.3389/frans.2025.1533486

The chemicalome profiling of Zishen Yuzhen Pill *in vivo* and its promoting effect on osteogenic differentiation of MC3T3-E1 cells

Juanjuan Cheng[1†], Xinyue Meng[2†], Daozheng Fang[2], Yong Zhu[2], Zhihao Liu[2], Xinyue Li[2], Ke Jie[3,4,5], Shiying Huang[1], Huilin Li[1], Shangbin Zhang[1], Jihang Chen[2*] and Jianping Chen[1*]

[1]Shenzhen Key Laboratory of Hospital Chinese Medicine Preparation, Shenzhen Traditional Chinese Medicine Hospital, The Fourth Clinical Medical College of Guangzhou University of Chinese Medicine, Shenzhen, China, [2]Shenzhen Key Laboratory of Steroid Drug Discovery and Development, School of Medicine, The Chinese University of Hong Kong, Shenzhen, China, [3]The Eighth Clinical Medical College of Guangzhou University of Chinese Medicine, Foshan, China, [4]Foshan Hospital of Traditional Chinese Medicine, Foshan, China, [5]Guangzhou University of Chinese Medicine, Guangzhou, China

Zishen Yuzhen Pill (ZYP) is a Chinese herbal product developed by Shenzhen TCM Hospital, which have been frequently used to treat osteoporosis (OP). This study aimed to determine the major chemical components of ZYP and its prototype compounds and metabolites in rat biological samples, as well as explore the potential effect of ZYP-containing serum in MC3T3-E1 cells. UPLC-Q/TOF-MS was used to identify the chemical components. Then, ZYP was orally administered to rat, and samples of plasma, urine, feces, bile, and tissue were collected to identify prototype compounds and metabolites. The viability of MC3T3-E1 cells was evaluated using the CCK-8 method after treatment with various concentrations (2%, 4%, and 8%) of ZYP-containing serum. Following treatment of MC3T3-E1 cells with ZYP-containing serum, the activity of alkaline phosphatase (ALP) and Alizarin red S (ARS) were measured, and the levels of Runx2, Opn, Opg and Osterix were quantified using the qPCR and Western blot analysis. And cells were collected for RNA-seq analysis. Results indicated that a total 152 compounds were identified in ZYP, including flavonoids, iridoid, lignans, triterpene saponins, etc. Furthermore, we detected a total of 70 prototype components and 99 metabolites distributed in different tissues. In addition, ZYP-containing serum observably promoted osteogenesis by increasing ALP and ARS activities, as well as up-regulating the expression of Runx2, Opn, Opg and Osterix in MC3T3-E1 cells. RNA-seq results indicated that the beneficial effects may be related to the upregulation of mitochondrial oxidative

Abbreviations: ABR, Achyranthis Bidentatae Radix; ALP, alkaline phosphatase; AR, Astragali Radix; BP, biological process; CC, cellular component; CR Codonopsis Radix; DR, Drynariae Rhizoma; ECL, enhanced chemiluminescence; EF, Epimedii Folium; FBS, fetal bovine serum; MF, molecular function; NRR, Notoginseng Radix Et Rhizoma; OD, Os Draconis; OP, osteoporosis; PBS, phosphate-buffered saline; OS, Oyster Shell; PR, Polygonati Rhizoma; Q/TOF-MS, quadrupole time-of-flight mass spectrometry; RR, Rehmanniae Radix; SCF, Schisandrae Chinensis Fructus; TCM, Traditional Chinese medicine; TP, Tortoise Plastron; TS, Turtle Shell; UPLC, ultra-high performance liquid chromatography; ZYP, Zishen Yuzhen Pill.

phosphorylation. This work provided further support for the traditional application of ZYP in the treatment of OP. And this study can promote the further pharmacokinetic and pharmacological evaluation of ZYP.

KEYWORDS

Zishen Yuzhen Pill, UPLC-QTOF/MS, chemical characterization, osteoporosis, MC3T3-E1 cells

1 Introduction

Osteoporosis (OP) is defined by the World Health Organization (WHO) as "a chronic systemic bone disease." The main characteristic of this disease is the loss of bone mass and destruction of the microstructure of bone tissue, eventually leading to increased bone fragility and fracture (Liu et al., 2019). OP is a major cause of fractures and can lead to persistent pain and serious injury in patients. Approximately 200 million people worldwide suffer from OP, causing around 8.9 million fractures annually. The medical cost of surgery-related fractures in China alone is predicted to reach $25.4 billion by 2050, nearly a 30-fold increase from 2010 (Si et al., 2015). There is no doubt that the prevention and treatment of OP is a public health challenge faced by the entire human population. Despite significant progress in the prevention and treatment of OP, current therapies have major limitations and adverse effects. Newly developed drugs are often expensive, limiting their widespread clinical use (Clynes et al., 2020). Additionally, adverse drug reactions, such as gastrointestinal issues, can affect patient compliance (Iolascon et al., 2020). Therefore, it is urgent to explore more effective and safer therapeutic drugs to overcome the treatment deadlock.

Traditional Chinese medicine (TCM) has been recognized as an integral part of modern medicine, serving as a vital resource of natural medicines and playing a significant role in the treatment of OP. The distinctive characteristic of TCM preparations is the use of multiple herbs, which contain numerous active ingredients that work synergistically on various targets to treat diseases, thereby enhancing the therapeutic effects and minimizing toxicity. In the theoretical system of traditional Chinese medicine (TCM), OP is called "*Gu Wei,*" which refers to the bone loss caused by kidney deficiency. Zishen Yuzhen Pill (ZYP), formerly known as Zishen Jiangtang Pill, is a Chinese herbal product developed by Professor Li Huilin of Shenzhen TCM Hospital, which has controllable quality, convenient administration, exact curative effect and independent intellectual property rights. It consists of 14 herbs, including Astragali Radix (AR), Achyranthis Bidentatae Radix (ABR), Codonopsis Radix (CR), Rehmanniae Radix (RR), Drynariae Rhizoma (DR), Schisandrae Chinensis Fructus (SCF), Epimedii Folium (EF), Polygonati Rhizoma (PR), Notoginseng Radix Et Rhizoma (NRR), Tortoise Plastron (TP), Turtle Shell (TS), Os Draconis (OD) and Oyster Shell (OS) (Li et al., 2018). Based on the theory of "kidney dominating bone," this prescription selects the products filled with lean marrow, which has the effect of tonifying Qi and nourishing Yin, nourishing the kidneys and strengthen bones. For over 20 years, it has a solid therapeutic foundation in clinical use to maintain blood glucose level and bone density. Previous studies indicated that ZYP can effectively improve abnormal bone metabolism in rat (Chu et al., 2021; Li et al., 2018). Moreover, ZYP also inhibited the adipocytes differentiate of mouse bone marrow mesenchymal stem cells, upregulation of RUNX2 and BMP-2 genes promotes osteogenic differentiation of BMSCs, and exerts multi-target anti-OP effects (Guo et al., 2011). However, a detailed analysis of the chemical composition of an ZYP remain unclear. In addition, the potential effect of ZYP on osteogenic differentiation in MC3T3-E1 cells is unknown. Therefore, it is crucial to systematically elucidate the chemical compositions and metabolite profiles of ZYP, particularly the qualitative identification and dynamic changes in the effective compounds *in vivo*. It is very important for us to better understand the bioactive ingredients responsible for the pharmacological effect of ZYP and provide a scientific basis for elucidating the substance basis of its therapeutic effect on OP.

Up to date, many modern analytical techniques have been used to explore the chemical composition of TCM. And with the application of mass spectrometers with high resolution, high sensitivity, and high mass accuracy, the identification level of various compounds of TCM has been greatly improved. It is well known that the use of ultra-high performance liquid chromatography (UPLC) for rapid separation of complex compounds in traditional Chinese medicine, and the use of quadrupole time-of-flight mass spectrometry (Q/TOF-MS) to obtain accurate structural characterization. The UPLC-QTOF/MS analytical method can help to fully explore the bioactive components, metabolites, and metabolic pathways of the TCM formulations after absorption by the human body (Ren et al., 2022; Yuan et al., 2024). The results will provide a powerful approach for the analysis of TCM or biological samples and deepen our understanding of the therapeutic effects of herbal preparations (Liu et al., 2017; Mi et al., 2019; Xiao et al., 2018). The major herb SCF in the formulation has been identified with 43 compounds by UPLC-QTOF/MS (Mu et al., 2022). There are still significant gaps in the understanding of ZYP bioactive components and *in vivo* metabolic pathways, especially its role in specific tissues. Therefore, it is important to establish a reliable methodology to overcome these problems.

In this study, we aim to analyze the chemical compounds of ZYP and the metabolic profile of the serum via UPLC-Q/TOF-MS. And the prototype compounds and potential metabolites identified were assessed using a semiquantitative method to investigate the potential therapeutic compounds of ZYP. Moreover, we also evaluate the effect of ZYP on MC3T3-E1 cell to provide new evidence for the anti-OP effect of ZYP.

2 Materials and methods

2.1 Chemicals and reagents

ZYP were obtained from the Pharmacy Department of Shenzhen TCM Hospital [Approval number: Guangdong Pharmaceutical Preparation Z20070083]. Its specific formula composition and preparation method refer to our previous

reports (Chen et al., 2019). Formic acid (FA), methanol (HPLC grade), and acetonitrile (HPLC grade) were purchased from Thermo Fisher Scientific (Waltham, MA, United States). Ultrapure deionized water was obtained from a Unique-R20 water-purification system (Xiamen, China). MC3T3-E1 cells were purchased from Procell Life Science and Technology Company (Cat# CL-0378, Wuhan, China). Ultrapure deionized water was obtained from a Unique-R20 water-purification system (Xiamen, China).

β-glycerophosphate sodium (#G9422), ascorbic acid (#A4403) and dexamethasone (#D4902) were purchased from Sigma-Aldrich (St. Louis, MO, United States). α-MEM media, fetal bovine serum (FBS) and phosphate-buffered saline (PBS) were purchased from Gibco (Grand Island, NY, United States). The Cell Counting Kit-8 (CCK-8, #C0037), alkaline phosphatase (ALP, #P0321) color development kit, Alizarin red S staining kit (ARS, #c0148), RNAeasy™ Animal RNA Isolation Kit (Beyotime, #R0027) and horseradish peroxidase (HRP)- conjugated goat anti-rabbit or goat anti-mouse antibody (#A0208 or #A0216), BeyoECL plus kit (#P0018) were obtained from Beyotime Biotechnology Co., (Jiangsu, China). Runx2 (#ab192256) and Osterix (#ab209484) primary antibody was purchased from Abcam (Cambridge, United Kingdom). Osteoprotegerin (OPG, #41289) primary antibodies was purchased from Signalway Antibody (CA, United States). Osteopontin (OPN, #22952) primary antibody was purchased from Proteintech company (Rosemont, IL, United States). β-actin (#3700) antibody was obtained from Cell Signaling Technology (Danvers, MA, United States). The PrimerScript RT reagent kit and SYBR qPCR Master Mix Kit were purchased from Vazyme (Biotech Co., Ltd., Nanjing, China).

2.2 Phytochemical analysis by UPLC-QTOF-MS

Phytochemical compounds were analyzed using Waters Acquity HSS T3 column (2.1 × 150 mm, 1.8 μm, Waters corporation, MA, United States) system. The mobile phase was a mixture of 0.1% formic acid in water (A) and acetonitrile (B), with an optimized gradient elution as follows: 0–5 min, 3%–8% B; 5–11 min, 8%–30% B; 11–20 min, 30%–80% B; 20–21 min, 80%–95% B; 21–27 min, 95%–95%. The injection volume was 2 μL, the column temperature was 35°C and flow rate was set at 0.30 mL/min. The MS analysis was performed using an X500B Q-TOF mass spectrometer (AB Sciex, Foster City, CA, United States). The MS data parameters were set as follows: the instrument was operated in positive (5.5 kV) or negative (−4.5 kV) ion mode, the full MS scan range was *m/z* 100–1,250. Then, some chemical components were identified by comparing with standard reference and an internal database (LibraryView). Others were identified by literature and online databases, such as MetaScope, ChemSpider and Progenesis QI software.

2.3 Animal

Specific pathogen-free male Sprague Dawley rats (SD, weighing 190–210 g) were provided by Beijing Vital River Laboratory Animal Technology Co., Ltd. The rats were housed in an animal facility with a standard 12 h light/dark cycle under constant temperature conditions and with free access to food and water. The experimental procedures were conducted in accordance with the Ethics Committees of the Chinese University of Hong Kong (Shenzhen, license number: CUHKSZ-AE2023014).

2.4 Rat treatment and sample collection

After 1 week of adaptive feeding, all rats were randomly divided into three groups: a control group for collecting blank bio-samples, ZYP -treated group (1.62 g/kg) for collecting plasma, urine, feces, and tissues, and ZYP -treated group (1.62 g/kg) for collecting bile. Rats in the control group were given normal saline by intragastric administration.

In different groups, blood samples were collected at 5, 15, 30, 60, 120, 240, 360, 480 and 600 min after intragastric administration and placed into heparin anticoagulant tubes. The tubes were then centrifuged at 4,500 rpm for 5 min to obtain plasma samples, which were combined for each time point and stored at −80°C until further analysis. Feces, urine and bile acid samples were collected from 0–600 min after administration, and collected every 120 min. After taking the above samples, rats were killed and the tissues were collected.

2.5 Sample preparation

After mixing 60 μL plasma (600 μL in total) at each time point, 1.8 mL ice acetonitrile was added. The sample was swirled for 2 min and centrifuged (at 13,000 rpm, 10 min, 4°C). Next, 400 μL of the supernatant was removed, and dry with nitrogen. The sample was redissolved with 200 μL 50% acetonitrile, centrifuged for 10 min at 13,000 rpm. 2 μL of the supernatant was analyzed by LC-MS.

A 0.3 g aliquot of tissue or feces sample were mixed with 1 mL methanol and homogenized six times for 30 s each time. The homogenate was centrifuged at 13,000 rpm for 10 min at 4°C. Next, 200 μL tissue supernatant dry with nitrogen. Redissolved with 200 μL 50% acetonitrile, centrifuged for 10 min at 13,000 rpm, which were then absorbed 2 μL supernatant to LC-MS.

Appropriate amount of urine/bile was centrifuged, centrifuged at 4,000 rpm for 10 min. Then, 1 mL of the supernatant was added to the activated C18 solid phase extraction column, washed with 1 mL of pure water, and then eluted with 1 mL of methanol. Finally, the eluent is collected. The MS/MS spectrum, Human Metabolome Database, METLIN database and literature data were used to identify metabolites.

2.6 Preparation of drug-containing serum

The prescribed dosage for ZYP was set at 18 g/d. Based on the dose equivalency conversion formula between humans and rat presented in the "Pharmacological Experimental Methodology," a dosage of 1.62 g/kg for ZYP was determined. Ten SD rats were administered with ZYP (0.81 g/kg) via intragastric administration twice a day to gain ZYP-containing serum, while another ten rats were treated with normal saline (10 mL/kg) to gain control serum. After treatment for 3 days, blood samples were collected and then subjected to centrifugation at 3,000 rpm for 10 min at 4°C. Finally, the collected supernatant was inactivated at 56°C for 30 min, sterilized through a 0.22 μm filter, and stored at −80°C for further use.

2.7 Cell culture

MC3T3-E1 cells were cultured in α-MEM supplemented with 10% FBS and 1% PS (100 U/mL penicillin and 100 μg/mL streptomycin) at 37°C, 5% CO_2. Subculturing of the cells was performed when they reached 80% confluence, and the medium was refreshed every 2 days. For induction of MC3T3-E1 osteogenic differentiation, the medium was added with 10 mM β-glycerophosphate sodium, 50 μg/L ascorbic acid and 100 μM dexamethasone. ALP staining was performed after 7 days of osteogenic differentiation. The medium was changed every 2 days.

2.8 Cell viability analysis and treatment

CCK-8 solution was used for the assessment of cell vitality following the instructions. 2×10^3 cells/well was maintained for the seeding of MC3T3-E1 cells in a 96-well plate for 24 h. Then, the cells were treated with different concentrations of drug-containing serum for 48 h. Cells were divided into the following groups: (1) Control group, (2) ZYP-treated group with 2%, 4% and 8% drug-containing serum, (3) Blank group with 8% control serum. After that, the working solution containing 10% CCK-8 reagent was added to each well and incubated for 1 h. The absorbance was measured at 450 nm with a multifunctional microplate reader.

2.9 ALP and ARS staining

After inducing osteogenic differentiation for 7 days or 21 days, the ALP and ARS staining in different treatment groups were performed according to the manufacturer's instructions of the corresponding assay kit. Briefly, the cells were fixed with 4% paraformaldehyde for 30 min. Then, cells were incubated with staining solution at room temperature for 18 h. After incubation, the cells were washed with PBS, and the stained cells were observed under a microscope immediately.

2.10 qRT-PCR

Total RNA was isolated from MC3T3-E1 cells using RNAeasy™ Animal RNA Isolation Kit. Then, RNA was utilized to synthesize cDNA following the manufacturer's guide. The result of qRT-PCR was analyzed by CFX 96 system (Version 3.1, Bio-Rad Corporation, CA, United States) by using SYBR qPCR Master Mix Kit. The gene expression level was calculated based on the $2^{-\triangle\triangle Ct}$ method and *β-actin* was used as a housekeeping gene. The primer sequences were listed in Table 1.

TABLE 1 Primer sequences.

Gene		Sequence (5′ to 3′)
Mouse-Runx2	Forward	ACTTCGTCAGCATCCTATCAGTTCC
	Reverse	CGTCAGCGTCAACACCATCATTC
Mouse-Opn	Forward	AAGAGCGGTGAGTCTAAGGAGTCC
	Reverse	TGGCTGCCCTTTCCGTTGTTG
Mouse-Opg	Forward	CCCTTGCCCTGACCACTCTTATAC
	Reverse	CCCTTCCTCACACTCACACACTC
Mouse-Osterix	Forward	TCGTCTGACTGCCTGCCTAGTG
	Reverse	CTGCGTGGATGCCTGCCTTG
Mouse-β-actin	Forward	CTGAGAGGGAAATCGTGCGTGAC
	Reverse	ACCGCTCGTTGCCAATAGTGATG

2.11 Western blot

In brief, cells were lysed in RIPA with 1% PMSF for 25 min, and then centrifuged at 12,000 rpm for 15 min at 4°C. Following that, equal protein (20 μg) was separated using 10% SDS-PAGE and blotted to a PVDF membrane. After transfer, the membrane was blocked with 5% skimmed milk for 1 h and then the following diluted primary antibodies were added at 4°C overnight: anti-Runx2 (1:1,000), anti-OPN (1:2,000), anti-OPG (1:1,000), anti-Osterix (1:1,000), anti-β-actin (1:1,000). Thereafter, the membranes were then incubated with HRP-conjugated goat anti-rabbit or anti-mouse antibody (1:5,000) at room temperature for 50 min. Finally, the chemiluminescence of target protein bands were performed with the enhanced chemiluminescence (ECL) detection system (ProteinSimple, San Jose, CA, United States).

2.12 RNA-sequencing

After induction of osteoblast differentiation for 2 days, total RNA from MC3T3-E1 cells was extracted by utilizing Trizol reagent. The RNA-sequencing analysis was conducted and analyzed. Briefly, the extracted RNA was evaluated for quality and integrity, and library preparation was conducted. Differential expression analysis between two groups was performed by employing the DESeq2 R package. Genes with FDR <0.05 and $|\log2(\text{foldchange})| \geq 1$ found by DESeq2 were regarded as differentially expressed genes (DEGs). KOBAS software was employed to test the statistical enrichment of DEGs in KEGG pathways.

2.13 Statistical analysis

All values are expressed as mean ± SD (standard deviation). Statistical difference was evaluated using one-way analysis of variance (ANOVA) followed by Tukey's test (GraphPad Pro Prism 8.0, San Diego, CA). $P < 0.05$ was considered statistically significant.

3 Results

3.1 Identification the main constituents of ZYP by UPLC-QTOF-MS/MS

As shown in Figures 1A, B, there was the representative base peak chromatogram (BPC) of ZYP in the positive and negative-ion scan. Based on the structural analysis and identification strategy of UPLC-QTOF/MS, the unknown components were classified

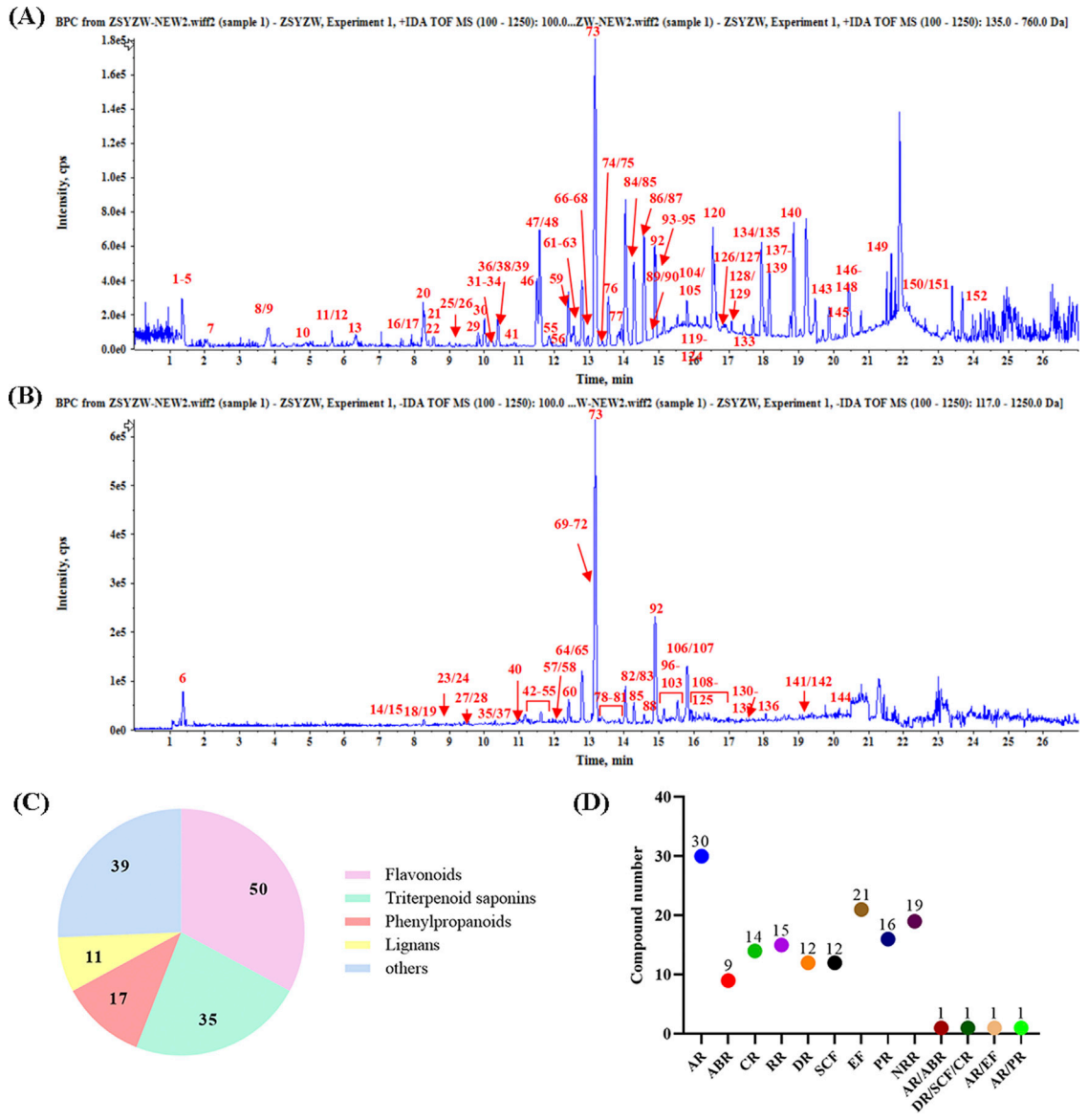

FIGURE 1
Base peak chromatogram (BPC) of ZYP. **(A)** Positive-ion scan. **(B)** Negative-ion scan. **(C)** Structural classification of compounds contained in ZYP. **(D)** The number of chemical components for each herb.

according to the fragmenting rules and diagnostic ions of different structural types of components. A total of 152 compounds were firstly tentatively identified from identified in ZYP, including 50 flavonoids, 35 triterpenoid saponins, 17 phenylpropanoids, 11 lignans, and 14 others (Figure 1C). The herbs and the number of their components are further summarized in Figure 1D (AR 30, ABR 9, CR 14, RR 15, DR 12, SCF 12, EF 21, PR 16, NRR 19, AR/ABR 1, DR/SCF/CR 1, AR/EF 1, and AR/PR 1). The details of these compounds were listed in Supplementary Table S1.

Subsequently, fifteen chemical components were accurately identified in CR, including amino acids, nucleosides, alkaloids, and glycosides, such as codonopsis. RR also contains fifteen chemical components, with characteristic components including iridoid, phenylpropanoid, and polysaccharides. DR was found to be rich in thirteen compounds, including flavonoids and phenylpropanoids, with naringin as its representative component. Seventeen compounds were identified in PR, with main components being flavonoids such as puerarin and luteolin. Results showed that AR was rich in thirty-three compounds, mainly flavonoids like mullein isoflavones and triterpenoid saponins such as astragalus saponins. Ten compounds were identified from ABR, mainly steroids and saponins. A total of nineteen compounds were identified in NRR, characterized by triterpenoid saponins, especially ginsenosides. Thirteen compounds were identified from SCF, with lignans as the characteristic components. A total of twenty-two flavonoids, such as icariin, were identified as the characteristic components of EF. The representative structures of each herb are depicted in Figure 2.

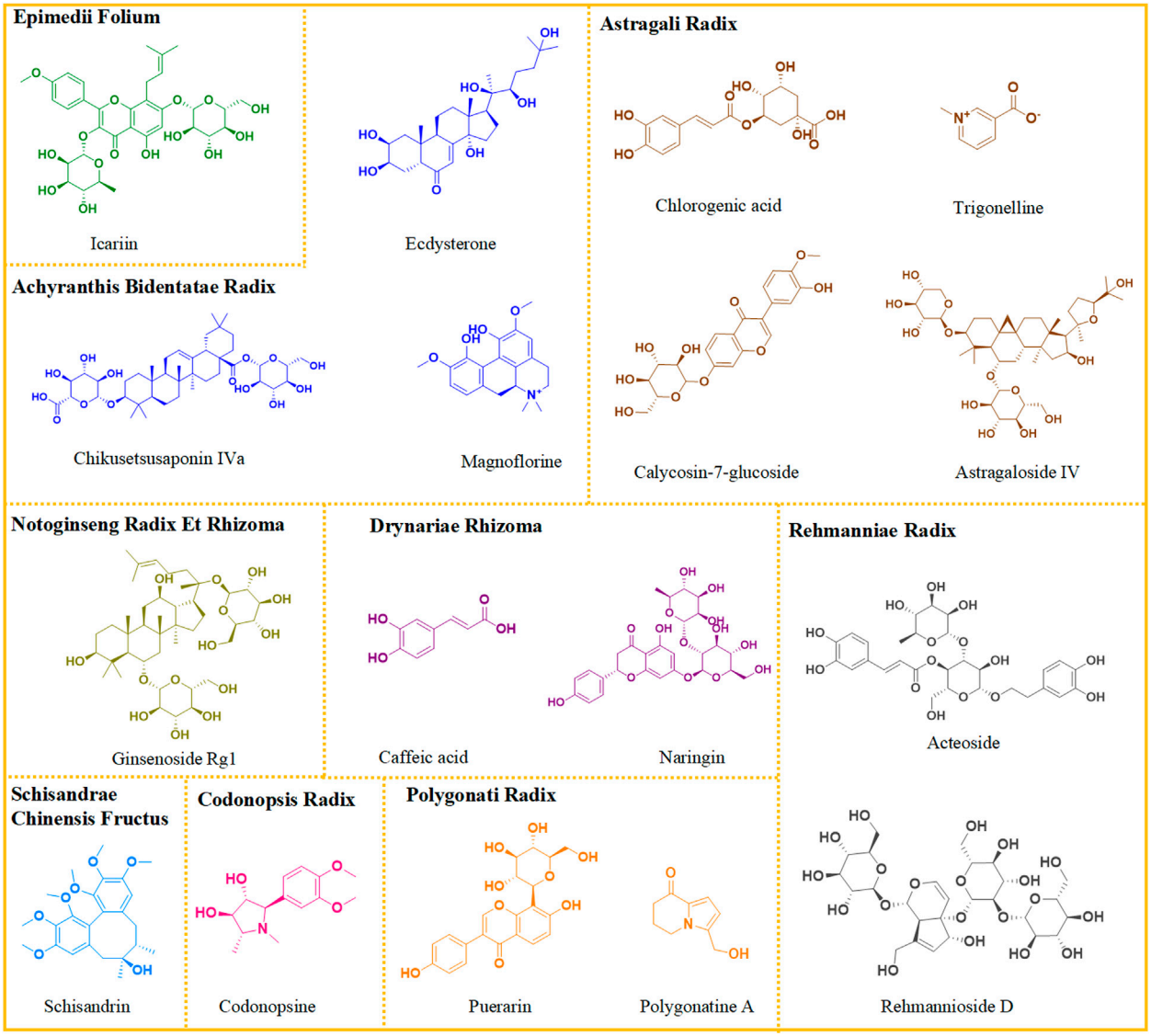

FIGURE 2
Representative chemical structures of each medicine in ZYP.

3.2 The mass spectrometry of characteristic compounds

According to the typical characteristic compounds, the secondary fragmentation and cracking behavior presented by secondary mass spectra were analyzed.

3.2.1 Alkaloid

Trigonelline, codonopsine, polygonatine and magnoflorine belong to categories of pyridine alkaloids, pyrrolidine alkaloids, indole alkaloids, and isoquinoline alkaloids, respectively. Alkaloids generally exhibit a good response in the positive ion mode, and the fragmentation typically occurs at the N-C junction. For example, the molecular ion peak of Magnoflorine in the mass spectrum is $[M]^+$ m/z 342.1699. In the secondary mass spectrum, the fragments m/z 299–297 are produced by cleavage at the N-heterocyclic site, and the fragment m/z 265 is formed by the further loss of CH_2O. Additional removal of CO generates the fragment m/z 237, and the fragment m/z 58 corresponds to the N-heterocyclic fragment $C_3H_8N^+$. The fragmentation pattern and secondary spectra are shown in Figure 3A.

3.2.2 Phenylpropanoids compounds

Phenylpropanoid compounds have the structural characteristics of C6-C3. Chlorogenic acid serves as an example to explain its fragmentation pattern. As shown in Figure 3B, the fragments are mainly formed by the cleavage of caffeoyl and quinic acid. The parent ion of chlorogenic acid is $[M-H]^-$ *m/z* 353.0879/$[M+H]^+$ *m/z* 355.1028. In the positive ion mode, the loss of one caffeoyl group produces the ion m/z 191. The continued removal of the caffeoyl group results in m/z 191, or the removal of the quinic acid part produces the ion m/z 179. Further removal of a CO_2 molecule generates the ion m/z 135.

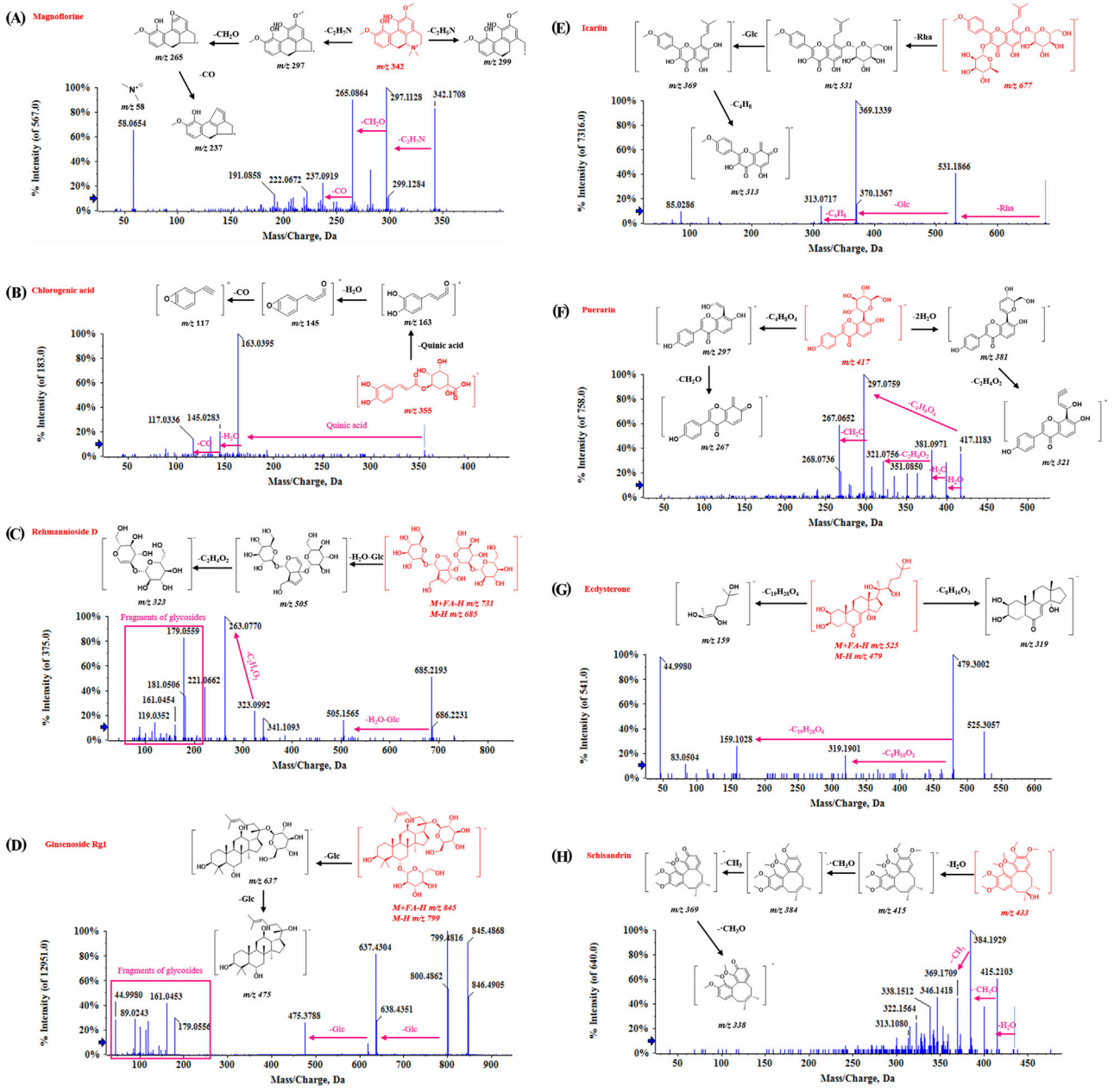

FIGURE 3
The mass spectrometry of characteristic compounds in ZYP. **(A)** Magnoflorine. **(B)** Chlorogenic acid. **(C)** Rehmannioside D. **(D)** Ginsenoside Rg1. **(E)** Icariin. **(F)** Puerarin. **(G)** Ecdysterone. **(H)** Schisandrin.

3.2.3 Iridoid terpenoids compounds

The iridoid terpenoids identified in the compound were derived from RR. Take Rehmannioside D, a characteristic compound in RR as an example, the parent ion was $[M+FA-H]^-$ *m/z* 731.2252, and $[M-H]^-$ *m/z* 685 could be observed in the secondary mass spectrometry. The loss of one molecule of water and one molecule of glucose produces a fragment at m/z 505. The disaccharide part generates fragments at *m/z* 323, and the neutral loss of $C_2H_4O_2$ results in fragments at *m/z* 263. In addition, fragments produced by the cleavage of other sugar residues, such as *m/z* 179 and 119, can be observed. The fragmentation pattern and secondary spectra are shown in Figure 3C.

3.2.4 Triterpenoid saponins compounds

Triterpenoid saponins are abundant in ZYP, as well as in NRR, AR, and ABR. The fragmentation patterns of saponins are consistent, with sequential glycoside cleavage commonly observed in secondary mass spectrometry. For example, the Ginsenoside Rg1, the parent ion has $[M+FA-H]^-$ at *m/z* of 845.4899. Its secondary mass spectrometry shows $[M-H]^-$ at m/z 799, with fragments at m/z 637 and m/z 475 resulting from the sequential removal of two glucose molecules (162 Da each). In addition, fragments at m/z 619 are produced by dehydration of hydroxyl groups on aglycones, and fragments at m/z 179, 161, 119, and 89 are generated from sugar residues. The fragmentation patterns and secondary spectra are illustrated in Figure 3D.

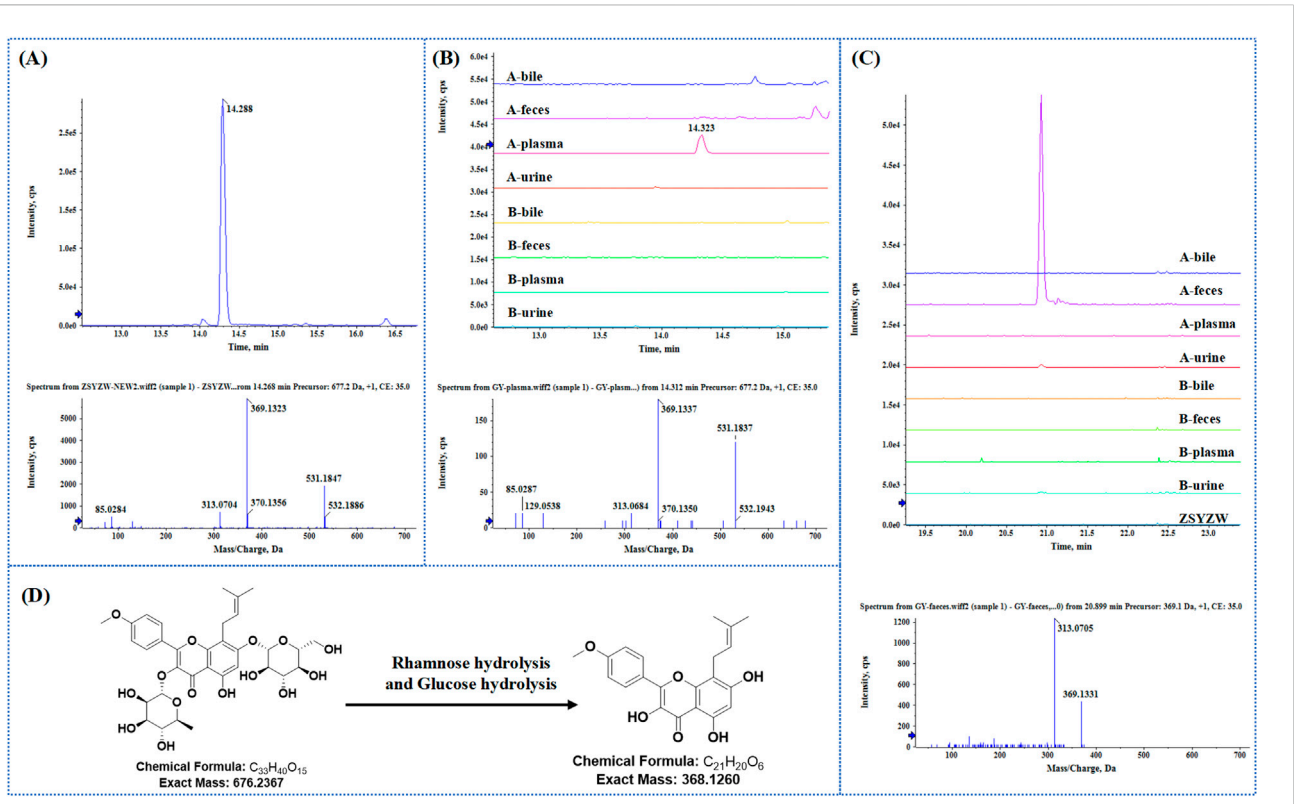

FIGURE 4
NO.85 Icariin was taken as an example to identify the prototype and metabolite in bio-samples. **(A)** Extraction ion flow and secondary mass spectrometry of Icariin in ZYP. **(B)** The superposition of Icariin in each biological sample extraction ion flow diagram and secondary mass spectrometry of administered plasma. **(C)** The superposition of M69 in ZYP and various biological samples extracted ion flow diagram and secondary mass spectrometry in the administered feces. **(D)** Examples of Icariin-M69 structural formulas and biotransformation pathways.

3.2.5 Flavonoids compounds

There are many kinds of flavonoids in ZYP, primarily derived from licorice. Flavonoids can be categorized based on their aglycones into flavanones, flavonoids, and flavonols. They can also be commonly substituted by oxosides, carbosides, and glucuronides, depending on the glycoside types. Regardless of the flavonoid type, desugar cleavage is common (e.g., oxoside losses of 162 Da, 146 Da, 176 Da, and carboside losses of 30 Da, 60 Da, 120 Da). Additionally, retro-Diels-Alder (RDA) cleavage occurs on aglycones. Icariin and Puerarin were used to illustrate the regularity of flavonoid cleavage in our results. Icariin, a flavonoside, shows distinct daughter ion peaks at m/z 531 and m/z 369 following the loss of −Rha (147 Da) and −Glc (162 Da). Icariin also forms a fragment at m/z 313 after the A-ring side chain is removed. Puerarin, a flavonoid glycoside, exhibits dehydration peaks and characteristic neutral losses of glycosides in secondary mass spectrometry. The fragmentation patterns and secondary spectra are shown in Figures 3E, F.

3.2.6 Steroid compounds

The steroids identified in ZYP are mainly derived from ABR, with ecdysterone being the characteristic component. Ecdysterone shows responses in both positive and negative ion modes. In its secondary mass spectrometry, numerous dehydration peaks are observed, such as m/z 445 and m/z 427. In the negative ion mode, the fragments m/z 319 and m/z 159 produced by the cracking of the group at position 17 can be very clearly observed. The fragmentation patterns are illustrated in Figure 3G.

3.2.7 Lignans compounds

The lignans identified in ZYP are primarily derived from SCF. For instance, in Schisandrin, the loss of methyl and methoxy groups from the benzene ring is common in secondary fragments. The fragmentation patterns are illustrated in Figure 3H.

3.3 Basic characterization of chemical substances in ZYP within biological samples of rats

Based on the chemical characterization of ZYP, the MS^2 fragments and retention time were used to analyze its components in plasma, urine, feces, and bile. Icariin (**85**) was selected as an example. As shown in Figure 4A, the extracted ion chromatogram (XIC) and secondary spectrum of icariin (RT 14.29 min, $[M+FA-H]^-$ *m/z* 721.2343 $[M+H]^+$ *m/z* 677.2435) in the extraction solution revealed characteristic fragments at m/z 531, 369, and 313. Figure 4B shows the superimposed XIC of Icariin in bile, feces, plasma, and urine from both administered and blank groups. The results indicated that Icariin responded only in the administered plasma at the corresponding retention time (with no response in blank samples), and the primary ppm met the requirements (<10 ppm). The secondary spectra were highly similar to those of Icariin in the extraction solution, with consistent secondary fragments (m/z 531, 369, 313), indicating

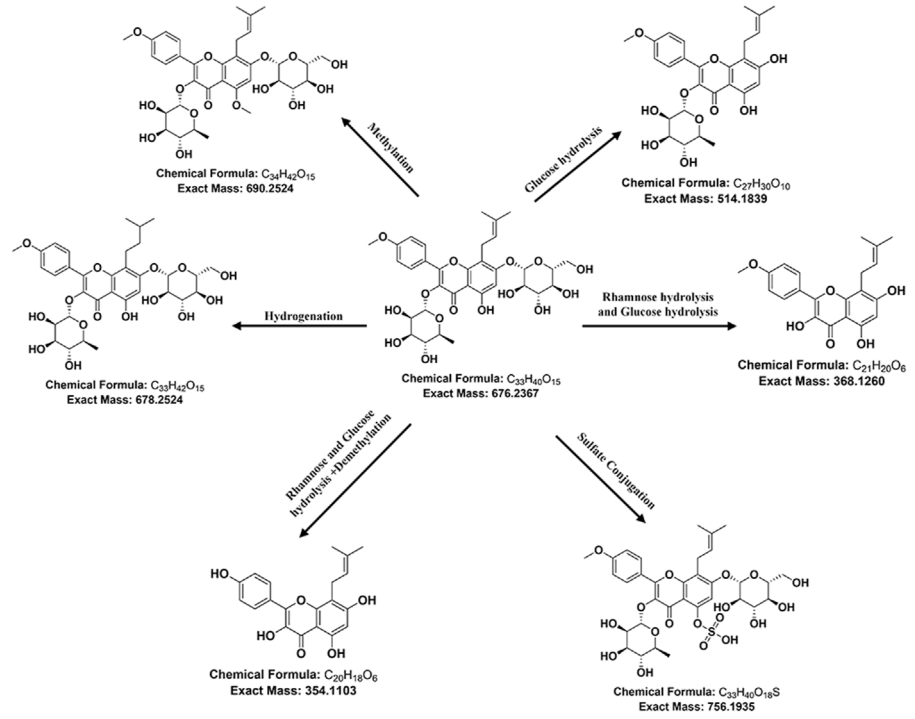

FIGURE 5
Icariin-related metabolite correlation diagram.

that Icariin can be absorbed into the blood and remain in the body to exert its effects.

Based on the phase I and phase II metabolism patterns and the similarity of the secondary mass spectrum profiles, metabolite libraries distinct from the prototype components can be quickly screened from the matrix. These metabolites are then automatically matched with the prototype components to assist in their identification and annotation. For example, the mass deviation between Icariin and M69 (m/z 369.1331, RT 20.93 min) was Δm = 308.1107, consistent with the molecular weight loss of Rhamnose and Glucose. This biological transformation pathway conforms to "Rhamnose hydrolysis and Glucose hydrolysis." The XIC superposition of M69 in each sample, as shown in Figure 4C, indicated a weak response in urine, but its chromatogram m/z was 369.1513 with ppm >10. The secondary profile of M69 in administered feces was similar to Icariin, with consistent fragments, including m/z 369 and m/z 313, indicating that M69 is a metabolite of Icariin. Additionally, M69's response in stool suggests it may be metabolized by intestinal flora. Figure 4D shows the structural formula of Icariin-M69. Following this principle, a total of six metabolites were matched to Icariin, and their structural association diagrams are presented in Figure 5.

3.4 Tissue distribution of prototypes and metabolites in ZYP

A total of 110, 65, 63, 59, 27 compounds were extracted from feces, plasma, urine, intestine and colon, respectively. And 70 compounds were detected in other tissues (Figure 6A). In detail, 70 prototype compounds were extracted from plasma, urine, feces, or bile (Figure 6B). Among them, 41 were detected in plasma, 25 in urine, 48 in feces, and 1 in bile. Further analysis of these prototype compounds revealed a total of 99 matched metabolites, with 24 detectable in plasma, 38 in urine, 62 in feces, and 3 in bile (Figure 6C). The tissue distribution of these compounds indicated that both prototypes and metabolites could be detected in various tissues, particularly in the intestines, the primary organ for digestion and absorption. Specifically, 18 prototypes and 9 metabolites were detected in the colon, while 36 prototypes and 23 metabolites were detected in the small intestine. These findings suggest that ZYP's impact on overall host metabolism, through regulation of intestinal flora, may be a significant mechanism of action. The detailed distribution of prototypes and metabolites is presented in Supplementary Tables S2, S3, respectively.

Figure 7 illustrates the association network between the prototypes and their related metabolites. Metabolites detected in feces may be processed by intestinal flora, while those metabolized by the liver are detectable in bile, plasma, and urine. Detailed biotransformation and annotation of prototype and metabolite components are provided in Supplementary Table S4.

3.5 Effects of ZYP-containing serum on cell viability and osteogenic capability in MC3T3-E1 cells

Figure 8A is a simple cell study protocols. As shown in Figure 8B, ZYP-containing serum (2%, 4%, and 8%) and 8% blank serum exerted

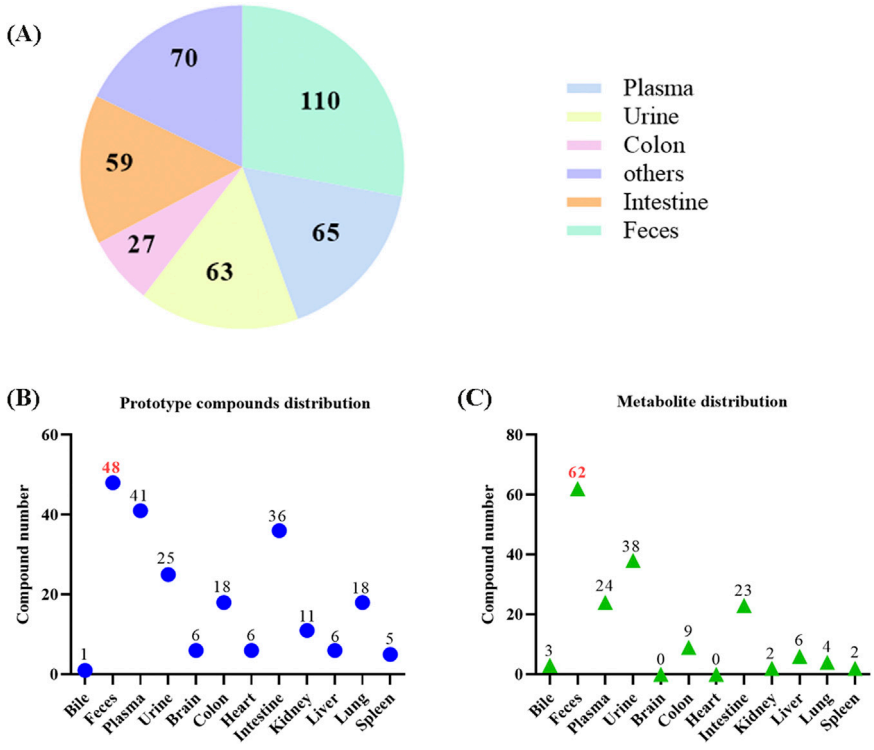

FIGURE 6
Tissue distribution of prototypes and metabolites in ZYP. **(A)** The number of components for each tissue. **(B)** The number of prototype compounds in different tissues. **(C)** The number of metabolite distribution in different tissues.

no obvious effect on the viability of MC3T3-E1 cells. In addition, we performed ALP staining to assess the osteogenic differentiation ability of MC3T3-E1 cells. Although the positive rate of ALP and ARS staining in 8% blank serum treated samples was similar to that of the control samples, our results showed that ZYP-containing serum treatment resulted in a higher rate of positive ALP and ARS staining in MC3T3-E1 cells compared to the control group (Figures 8C, D).

3.6 Effect of ZYP-containing serum on the expression levels of osteogenic differentiation-related proteins in MC3T3-E1 cells

The results revealed that the addition of 8% blank serum to MC3T3-E1 cells did not yield any noticeable differences in the mRNA and protein levels of Runx2, Opn, Opg and Osterix when compared with the control group. Conversely, the mRNA and protein levels of Runx2, Opn, Opg and Osterix were elevated by ZYP-containing serum at concentrations of 2%, 4%, and 8% in MC3T3-E1 cells when compared with the blank group (as depicted in Figure 9). Taken together, these findings suggest the role of ZYP-containing serum promotes the levels of osteogenic differentiation-related proteins in MC3T3-E1 cells.

3.7 ZYP-containing serum upregulate oxidative phosphorylation in the process of osteogenic differentiation in MC3T3-E1 cells

To elucidate the potential mechanism underlying the impact of ZYP-containing serum in promoting the osteogenic differentiation, RNA-seq analysis was further conducted. A total of 5,249 DEGs with 2,700 upregulated and 2,549 downregulated genes were confirmed between MC3T3-E1 treated with or without ZYP-containing serum (Figure 10A). Moreover, the heat map suggested that a set of genes (Cox5a, Cox7a2, Cox7c, Ndufa2, Ndufs8, Atp5g3, Atp5o, Atp5d, Ndufb5, Ndufa9, Ndufa12, Uqcrh, Ndufb7, Ndufb8, Ppa1, Ndufb10 and Ndufab1) of MC3T3-E1 were upregulated by ZYP-containing serum (Figure 10B).

The top 20 enriched KEGG pathways and GO terms (biological process (BP), cellular component (CC), molecular function (MF)) were shown in Figure 11. The results suggested that ZYP-containing serum significantly promoted osteogenic differentiation may be closely related to the upregulation of mitochondrial oxidative phosphorylation.

4 Discussion

OP is recognized as a serious public health problem worldwide. At present, the researchers are working to identify products with

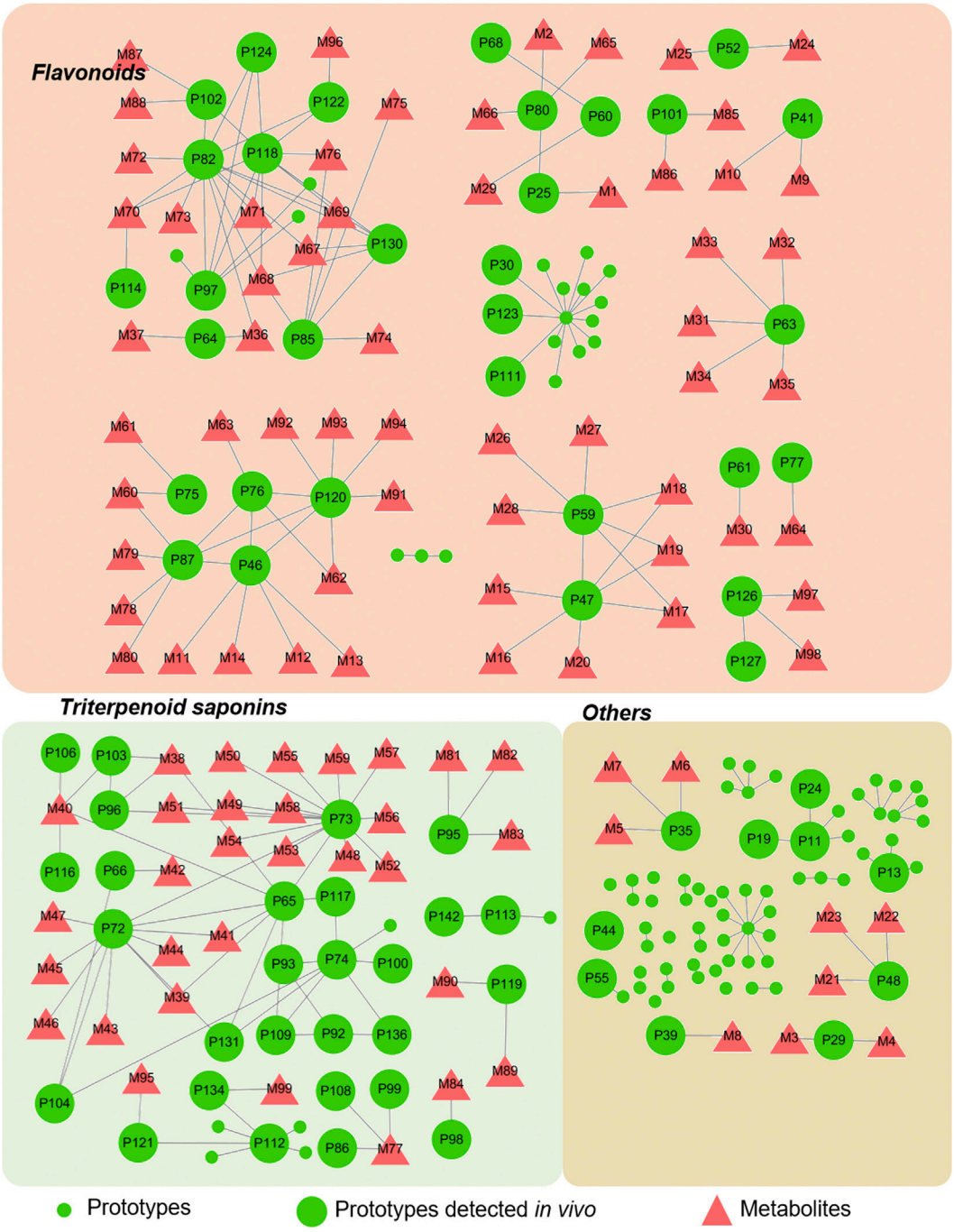

FIGURE 7
Correlation between prototype and metabolites.

reduced osteoclast absorption activity, namely anti-bone absorbents (Vasikaran et al., 2011). Clinically, estrogen, bisphosphonates, and other selective estrogen receptor modulators are widely used for the treatment of OP (Cosman et al., 2014). Unfortunately, these agents can produce some adverse effects, such as gastrointestinal distress, as well as osteonecrosis of jaw (Christenson et al., 2012; Weinstein, 2012; Otto et al., 2011). Natural products, especially the Chinese herbal medicine, offer a promising alternative treatment for maintaining bone health and preventing metabolic bone diseases (Putnam et al., 2007; An et al., 2016). ZYP is a TCM compound developed by Shenzhen TCM Hospital and widely used in the treatment of OP.

In this study, a high-sensitivity and high-resolution UPLC-QTOF-MS/MS method was used to determine the material basis of ZYP. To the best of our knowledge, this is the first comprehensive characterization of the chemical composition of ZYP. Through comparison with standards and literature references, 152 chemical compounds in ZYP were tentatively identified,

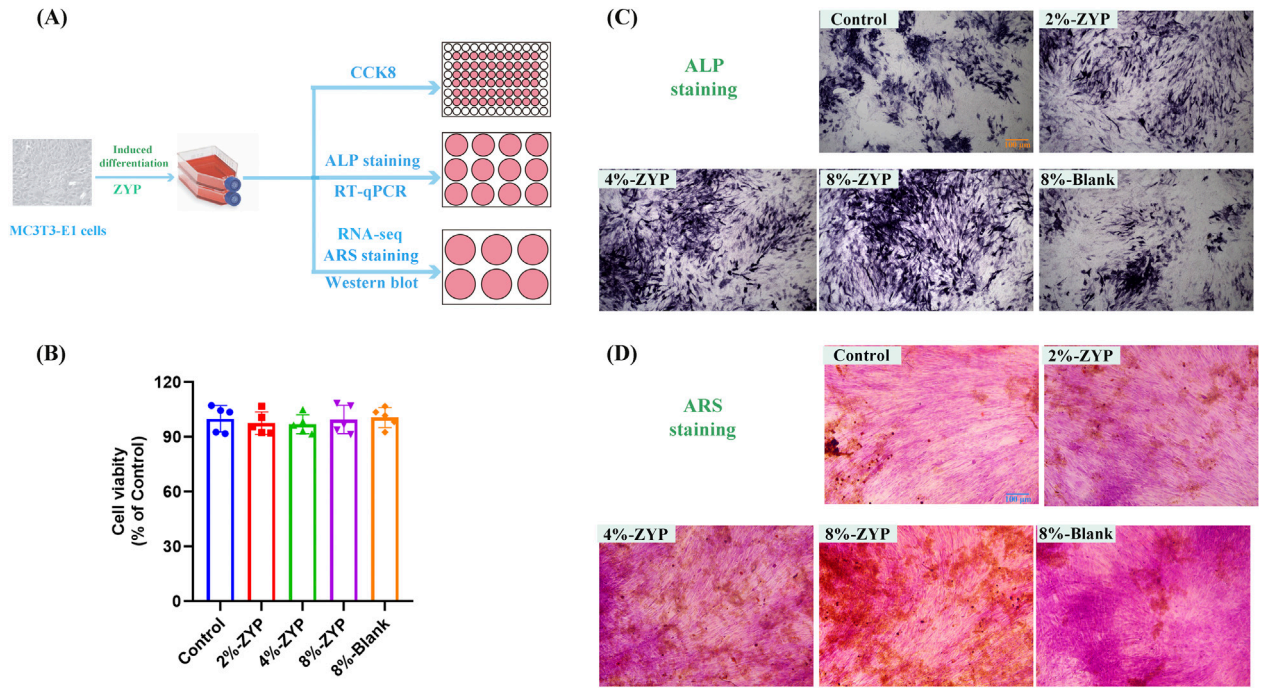

FIGURE 8
ZYP-containing serum improves osteogenic capability in differentially treated group. **(A)** Cell study protocols. **(B)** Cell viability of ZYP-containing serum in MC3T3-E1 cells. **(C)** Representative images showing ALP staining on the 7th day. **(D)** Representative images showing ARS staining on the 21st day.

including flavonoids, iridoids, lignans, triterpene saponins, and others. The composition of ZYP is complex, and after oral administration, these compounds are transformed within the organism, making the composition of exogenous small molecule compounds even more complicated.

Our results indicated the presence of a total of 70 prototype compounds of ZYP in plasma, urine, feces, and bile. Further analysis of these prototypes revealed 99 metabolites. To investigate the *in vivo* process of ZYP further, a tissue distribution study was performed. The results revealed that the compounds in ZYP had a wide distribution throughout the body. Notably, the tissue distribution showed that both prototypes and metabolites could be detected in various tissues, especially in the colon and intestine, which are crucial organs for digestion and absorption. Specifically, 27 compounds were detected in the colon, and 59 compounds were detected in the intestine. These results clearly indicated that intestinal flora may be one of the important pathways through which ZYP exerts its pharmacological effects.

It has been reported that many compounds found in the colon and intestine could ameliorate osteoporosis. For instance, **39** Magnoflorine has been shown to promote new osteoid formation and help restore the integrity of trabecular bone microstructures of the spinal canal, thus preventing the progression of osteoarthritis (Cai et al., 2018). Various flavonoid compounds, such as **52** Hyperoside (Chen et al., 2018; An et al., 2023), **59** Naringin (Wang et al., 2022; Li et al., 2014), **122** Sagittatoside B (Song et al., 2023), **124** 2-O-Rhamnosylicariside II (Zhao et al., 2016) and **130** Baohuoside I (Ma et al., 2022) could ameliorate development of osteoporosis through different mechanisms, including regulation of miR-19a-5p/IL-17A axis, inhibition of the TRAF-6 mediated RANKL/RANK/NF-kB pathway, elevation of the OPG/RANKL ratio, suppression of the JAK2/STAT3 pathway, regulation of immune functions and antioxidant activity. Additionally, triterpenoid saponins, such as **65** Notoginsenoside R1 (Wang et al., 2015; Li et al., 2021), **72** Ginsenoside Re (Kim et al., 2016; Park et al., 2016), **73** Ginsenoside Rg1 (Jiang et al., 2024; Chen et al., 2022), **92** Ginsenoside Rb1 (Cheng et al., 2012; Zhang et al., 2022; Ding et al., 2023), **100** Ginsenoside Rg2 (Lee et al., 2023), **113** Chikusetsusaponin Iva (Tao et al., 2019), **119** Soyasaponin Bb (Kim et al., 2019), **121** Astragaloside II (Kong et al., 2012) and **136** Ginsenoside Rg3 (Zhang et al., 2020; Song et al., 2020) have demonstrated therapeutic effects in improving osteoporosis. These findings provided theoretical support for the prevention and treatment of osteoporosis by ZYP.

MC3T3-E1 cells are derived from mouse embryonic osteoblast precursor cells. An osteogenic induction medium can promote the osteogenic differentiation of MC3T3-E1. Our results revealed that ZYP-containing serum significantly accelerates this process. ALP activity is the most widely recognized biochemical index of osteoblastic activity (Vimalraj, 2020), as it is atypical protein product of osteoblast phenotype and osteoblast differentiation. Runx2 plays a pivotal role in promoting osteogenesis by initiating the expression of osteogenic-specific matrix proteins, such as ALP and OCN (de Farias et al., 2023). OPN, a "bone-bridging" protein abundant in mineralized tissues, has long been involved in bone remodeling (Denhardt and Noda, 1998). Osterix is an osteoblast-specific transcription factor essential for cell differentiation, and its knockout results in an osteoporotic

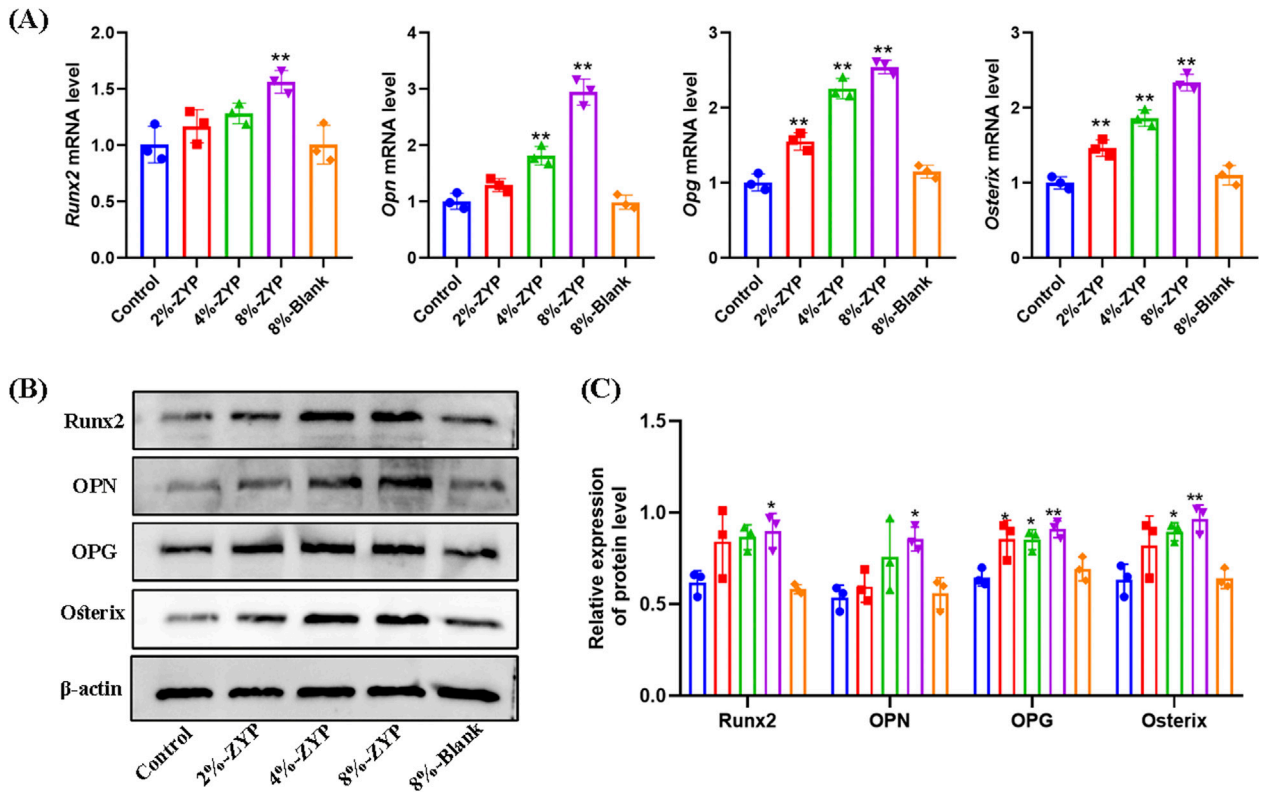

FIGURE 9
Effect of ZYP-containing serum on the expression profiles of osteogenesis associated proteins in MC3T3-E1 cells. **(A)** The mRNA expression of *Runx2*, *Opn*, *Opg* and *Osterix*. **(B)** Representative Western blotting images of Runx2, Opn, Opg and Osterix in different treatment groups. **(C)** Quantitative analysis of Runx2, Opn, Opg and Osterix protein expression levels. $*p < 0.05$, $**p < 0.01$ vs. Control group.

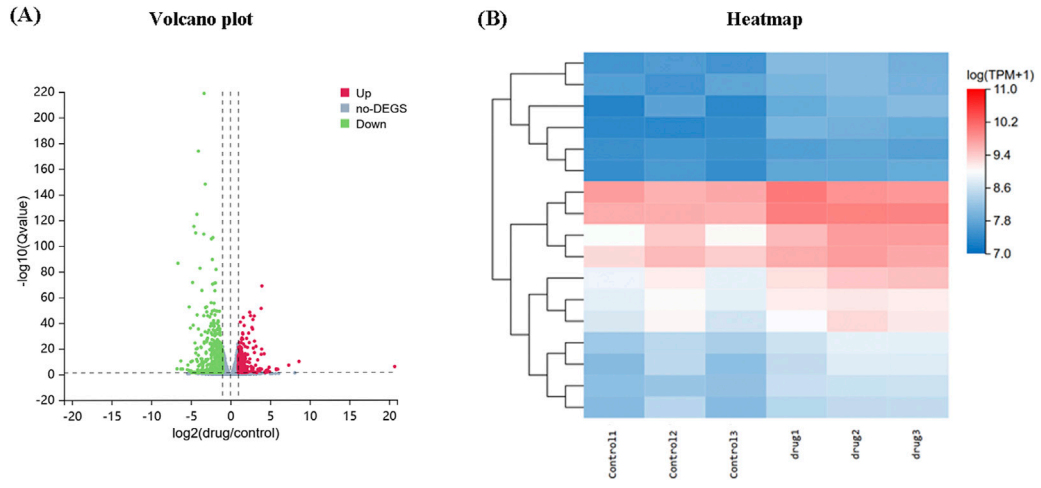

FIGURE 10
(A) Volcano plots of RNA-seq. **(B)** Heatmap of RNA-seq.

phenotype in bone growth due to reduced osteoblast function during bone formation (Sinha and Zhou, 2013; Baek et al., 2009). OPG, a potent osteoclast activation inhibitor, decreases the bone resorption capacity of osteoclasts and plays a regulatory role in bone mineral density (Lacey et al., 2000). These bone formation markers reflect the osteogenic ability of MC3T3-E1 cells.

Our present results indicated that ZYP-containing serum treatment resulted in a higher rate of positive ALP staining in

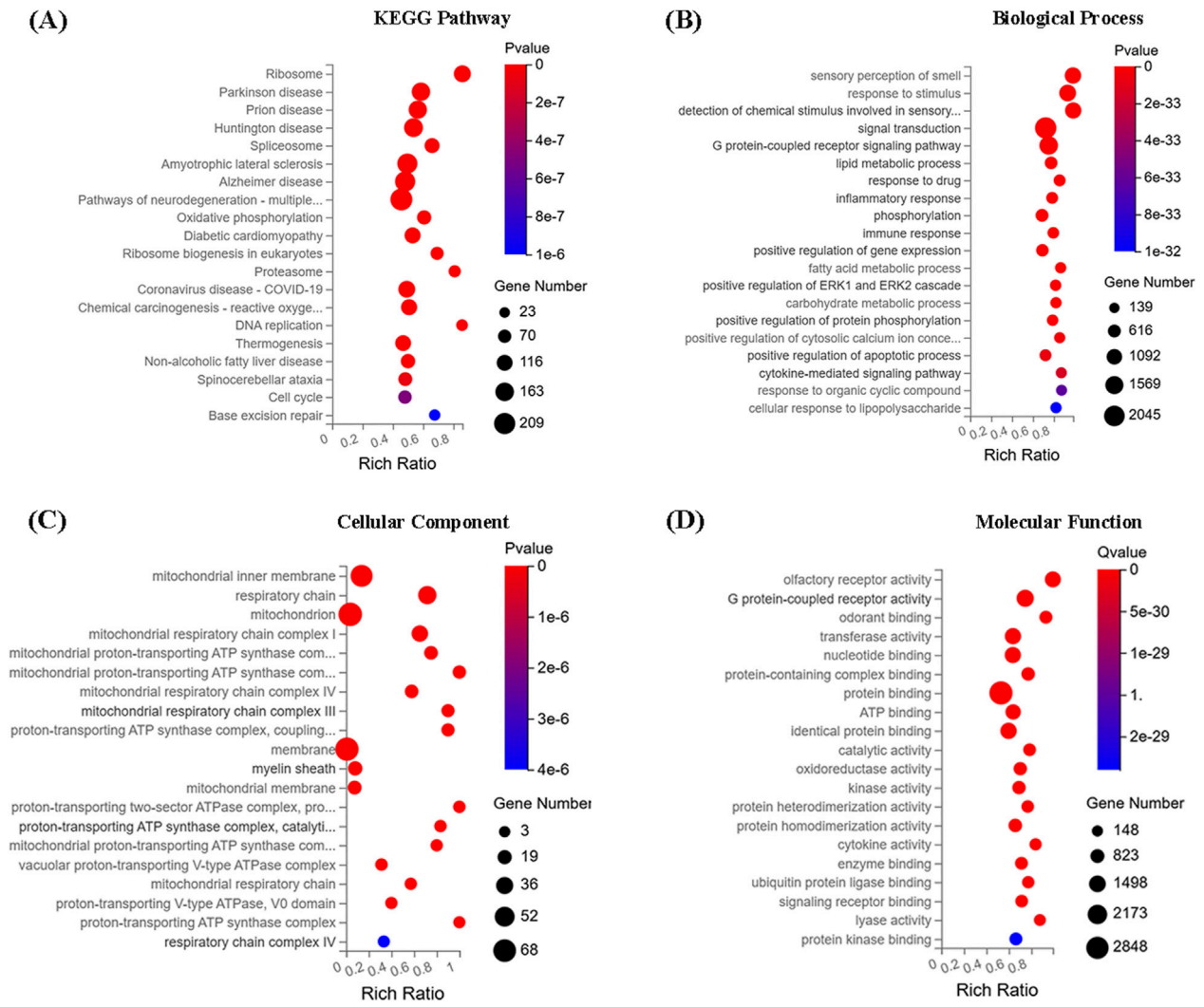

FIGURE 11
RNA-seq results. **(A)** KEGG function enrichment analysis. **(B)** GO function enrichment-biology process. **(C)** GO function enrichment-cell component. **(D)** GO function enrichment-molecular function.

MC3T3-E1 cells compared to the control group. The expression of Runx2, OPN, Osterix and OPG increased when MC3T3-E1 cells were treated with ZYP-containing serum, which suggested that ZYP-containing serum was actively involved in the early osteogenic differentiation and the late bone mineralization of osteoblasts. The mechanism may be related to the upregulation of mitochondrial oxidative phosphorylation, as indicated by RNA-seq analysis. Therefore, further investigation into the effect of this drug on the process of mitochondrial oxidative phosphorylation is necessary. In addition, the chemical composition of ZYP remains unclear.

The present study is the first to identify the chemical components in ZYP, which was important to determine whether prototypical compounds or metabolites involved in specific diseases. In addition, our results also indicated that ZYP-containing serum prominently promoted the osteogenic differentiation of MC3T3-E1. However, more efforts are merited to investigate the underlying mechanism and potential benefit of ZYP.

5 Conclusion

To summarize, UPLC-Q/TOF-MS was first applied for the characterization of the chemical compound of ZYP. Subsequently, prototype compounds and metabolites were identified after gavage of ZYP in rats. Moreover, the multi-compound pharmacokinetics strategy combined with semi-quantitative methods presented the dynamic changes in the prototypical compounds and metabolites *in vivo* by UPLC-Q/TOF-MS. This work provided a dependable and appropriate strategy for the screening and discovery of potentially bioactive ingredients that promote the pharmacological effects of TCM, laying a foundation for further in-depth studies on the bioactive ingredients of ZYP. In addition, the current study demonstrated ZYP-containing serum prominently promoted the osteogenic differentiation of MC3T3-E1. The possible mechanism may be related to the upregulation of mitochondrial oxidative phosphorylation.

Data availability statement

The datasets presented in this study can be found in online repositories. The names of the repository/repositories and accession number(s) can be found in the article/Supplementary Material.

Ethics statement

The animal study was approved by the Chinese University of Hong Kong. The study was conducted in accordance with the local legislation and institutional requirements.

Author contributions

JC: Conceptualization, Data curation, Formal Analysis, Investigation, Methodology, Project administration, Software, Writing–original draft. XM: Data curation, Investigation, Software, Writing–original draft. DF: Investigation, Project administration, Software, Writing–original draft. YZ: Investigation, Project administration, Software, Writing–original draft. ZL: Investigation, Methodology, Writing–original draft. XL: Investigation, Methodology, Writing–original draft. KJ: Investigation, Methodology, Writing–original draft. SH: Methodology, Visualization, Writing–original draft. HL: Conceptualization, Project administration, Writing–original draft. SZ: Conceptualization, Project administration, Writing–review and editing. JHC: Formal Analysis, Investigation, Project administration, Writing–review and editing. JPC: Conceptualization, Funding acquisition, Writing–review and editing.

Funding

The author(s) declare that financial support was received for the research, authorship, and/or publication of this article. This research was supported by the Sanming Project of Medicine in Shenzhen (SZZYSM202111002), Shenzhen Medical Research Fund (B2302008), Shenzhen Science and Technology Program (JSGG20210802093208023, JCYJ20220818103402006, JCYJ20210324140204011 and ZDSYS201606081515458), Foundation of Guangdong Provincial Key Laboratory of Functional Substances in Medicinal Edible Resources and Healthcare Products (No. GPKLFSHP202101), and Traditional Chinese Medicine Bureau of Guangdong Province (20231286).

Conflict of interest

The authors declare that the research was conducted in the absence of any commercial or financial relationships that could be construed as a potential conflict of interest.

Generative AI statement

The author(s) declare that no Generative AI was used in the creation of this manuscript.

Publisher's note

All claims expressed in this article are solely those of the authors and do not necessarily represent those of their affiliated organizations, or those of the publisher, the editors and the reviewers. Any product that may be evaluated in this article, or claim that may be made by its manufacturer, is not guaranteed or endorsed by the publisher.

Supplementary material

The Supplementary Material for this article can be found online at: https://www.frontiersin.org/articles/10.3389/frans.2025.1533486/full#supplementary-material

References

An, H., Chu, C., Zhang, Z., Zhang, Y., Wei, R., Wang, B., et al. (2023). Hyperoside alleviates postmenopausal osteoporosis via regulating miR-19a-5p/IL-17A axis. *Am. J. Reprod. Immunol.* 90 (1), e13709. doi:10.1111/aji.13709

An, J., Yang, H., Zhang, Q., Liu, C., Zhao, J., Zhang, L., et al. (2016). Natural products for treatment of osteoporosis: the effects and mechanisms on promoting osteoblast-mediated bone formation. *Life Sci.* 147, 46–58. doi:10.1016/j.lfs.2016.01.024

Baek, W. Y., Lee, M. A., Jung, J. W., Kim, S. Y., Akiyama, H., de Crombrugghe, B., et al. (2009). Positive regulation of adult bone formation by osteoblast-specific transcription factor osterix. *J. Bone. Min. Res.* 24 (6), 1055–1065. doi:10.1359/jbmr.081248

Cai, Z., Feng, Y., Li, C., Yang, K., Sun, T., Xu, L., et al. (2018). Magnoflorine with hyaluronic acid gel promotes subchondral bone regeneration and attenuates cartilage degeneration in early osteoarthritis. *Bone* 116, 266–278. doi:10.1016/j.bone.2018.08.015

Chen, J., Zheng, L., Hu, Z., Wang, F., Huang, S., Li, Z., et al. (2019). Metabolomics reveals effect of Zishen Jiangtang Pill, a Chinese Herbal product on high-fat diet-induced type 2 diabetes mellitus in mice. *Front. Pharmacol.* 10, 256. doi:10.3389/fphar.2019.00256

Chen, W., Jin, X., Wang, T., Bai, R., Shi, J., Jiang, Y., et al. (2022). Ginsenoside Rg1 interferes with the progression of diabetic osteoporosis by promoting type H angiogenesis modulating vasculogenic and osteogenic coupling. *Front. Pharmacol.* 13, 1010937. doi:10.3389/fphar.2022.1010937

Chen, Y., Dai, F., He, Y., Chen, Q., Xia, Q., Cheng, G., et al. (2018). Beneficial effects of hyperoside on bone metabolism in ovariectomized mice. *Biomed. Pharmacother.* 107, 1175–1182. doi:10.1016/j.biopha.2018.08.069

Cheng, B., Li, J., Du, J., Lv, X., Weng, L., and Ling, C. (2012). Ginsenoside Rb1 inhibits osteoclastogenesis by modulating NF-κB and MAPKs pathways. *Food. Chem. Toxicol.* 50 (5), 1610–1615. doi:10.1016/j.fct.2012.02.019

Christenson, E. S., Jiang, X., Kagan, R., and Schnatz, P. (2012). Osteoporosis management in post-menopausal women. *Minerva Ginecol.* 64 (3), 181–194.

Chu, S., Liu, D., Zhao, H., Shao, M., Liu, X., Qu, X., et al. (2021). Effects and mechanism of zishen Jiangtang Pill on diabetic osteoporosis rats based on proteomic analysis. *Evidence-based complementary Altern. Med. eCAM* 2021, 7383062. doi:10.1155/2021/7383062

Clynes, M. A., Harvey, N. C., Curtis, E. M., Fuggle, N. R., Dennison, E. M., and Cooper, C. (2020). The epidemiology of osteoporosis. *Br. Med. Bull.* 133 (1), 105–117. doi:10.1093/bmb/ldaa005

Cosman, F., de Beur, S. J., Leboff, M. S., Lewiecki, E. M., Tanner, B., Randall, S., et al. (2014). Clinician's guide to prevention and treatment of osteoporosis. *Osteoporos. Int.* 25 (10), 2359–2381. doi:10.1007/s00198-014-2794-2

de Farias, C. S., Garcez, A. S., Teixeira, L. N., and Suzuki, S. S. (2023). *In vitro* effects of photobiomodulation on cell migration and gene expression of ALP, COL-1, RUNX-2, and osterix in cementoblasts. *Lasers Med. Sci.* 38 (1), 121. doi:10.1007/s10103-023-03775-5

Denhardt, D. T., and Noda, M. (1998). Osteopontin expression and function: role in bone remodeling. *Cell. Biochem.* 72 (S30-31), 92–102. doi:10.1002/(SICI)1097-4644(1998)72:30/31+<92::AID-JCB13>3.0.CO;2-A

Ding, L., Gao, Z., Wu, S., Chen, C., Liu, Y., Wang, M., et al. (2023). Ginsenoside compound-K attenuates OVX-induced osteoporosis via the suppression of RANKL-induced osteoclastogenesis and oxidative stress. *Nat. Product. Bioprospecting.* 13 (1), 49. doi:10.1007/s13659-023-00405-z

Guo, B., Liu, Z., Zeng, B., Ling, Y., Xiao, Y., Chen, Z., et al. (2011). Efect of Zishen Jiangtang Pills on adipogenic diferentiation of mice MSC and its mechanisms. *China Pharm.* 22 (11), 985–987. (Chinese).

Iolascon, G., Moretti, A., Toro, G., Gimigliano, F., Liguori, S., and Paoletta, M. (2020). Pharmacological therapy of osteoporosis: what's new? *Clin. Interv. Aging.* 15, 485–491. doi:10.2147/CIA.S242038

Jiang, Z., Deng, L., Li, M., Alonge, E., Wang, Y., and Wang, Y. (2024). Ginsenoside Rg1 modulates PI3K/AKT pathway for enhanced osteogenesis via GPER. *Phytomedicine* 124, 155284. doi:10.1016/j.phymed.2023.155284

Kim, H. M., Kim, D. H., Han, H. J., Park, C. M., Ganipisetti, S. R., Valan, A. M., et al. (2016). Ginsenoside Re promotes osteoblast differentiation in mouse osteoblast precursor MC3T3-E1 cells and a zebrafish model. *Molecules* 22 (1), 42. doi:10.3390/molecules22010042

Kim, S. H., Yuk, H. J., Ryu, H. W., Oh, S. R., Song, D. Y., Lee, K. S., et al. (2019). Biofunctional soyasaponin Bb in peanut (*Arachis hypogaea* L.) sprouts enhances bone morphogenetic protein-2-dependent osteogenic differentiation via activation of runt-related transcription factor 2 in C2C12 cells. *Phytother. Res.* 33 (5), 1490–1500. doi:10.1002/ptr.6341

Kong, X. H., Niu, Y. B., Song, X. M., Zhao, D. D., Wang, J., Wu, X. L., et al. (2012). Astragaloside II induces osteogenic activities of osteoblasts through the bone morphogenetic protein-2/MAPK and Smad1/5/8 pathways. *Int. J. Mol. Med.* 29 (6), 1090–1098. doi:10.3892/ijmm.2012.941

Lacey, D. L., Tan, H. L., Lu, J., Kaufman, S., Van, G., Qiu, W., et al. (2000). Osteoprotegerin ligand modulates murine osteoclast survival *in vitro* and *in vivo*. *Am. J. Pathol.* 157 (2), 435–448. doi:10.1016/S0002-9440(10)64556-7

Lee, S. H., Park, S. Y., Kim, J. H., Kim, N., and Lee, J. (2023). Ginsenoside Rg2 inhibits osteoclastogenesis by downregulating the NFATc1, c-Fos, and MAPK pathways. *BMB Rep.* 56 (10), 551–556. doi:10.5483/BMBRep.2023-0100

Li, F., Sun, X., Ma, J., Ma, X., Zhao, B., Zhang, Y., et al. (2014). Naringin prevents ovariectomy-induced osteoporosis and promotes osteoclasts apoptosis through the mitochondria-mediated apoptosis pathway. *Biochem. Biophys. Res. Commun.* 452 (3), 629–635. doi:10.1016/j.bbrc.2014.08.117

Li, H., Chu, S., Zhao, H., Liu, D., Liu, X., Qu, X., et al. (2018). Effect of zishen Jiangtang Pill, a Chinese herbal product, on rats with diabetic osteoporosis. *Evidence-based complementary Altern. Med. eCAM* 2018, 7201914. doi:10.1155/2018/7201914

Li, X., Lin, H., Zhang, X., Jaspers, R. T., Yu, Q., Ji, Y., et al. (2021). Notoginsenoside R1 attenuates oxidative stress-induced osteoblast dysfunction through JNK signalling pathway. *J. Cell. Mol. Med.* 25 (24), 11278–11289. doi:10.1111/jcmm.17054

Liu, J., Curtis, E. M., Cooper, C., and Harvey, N. C. (2019). State of the art in osteoporosis risk assessment and treatment. *J. Endocrinol. Invest.* 42 (10), 1149–1164. doi:10.1007/s40618-019-01041-6

Liu, K., Song, Y., Liu, Y., Peng, M., Li, H., Li, X., et al. (2017). An integrated strategy using UPLC-QTOF-MS(E) and UPLC-QTOF-MRM (enhanced target) for pharmacokinetics study of wine processed Schisandra Chinensis fructus in rats. *J. Pharm. Biomed. Anal.* 139, 165–178. doi:10.1016/j.jpba.2017.02.043

Ma, M., Fan, A. Y., Liu, Z., Yang, L. Q., Huang, J. M., Pang, Z. Y., et al. (2022). Baohuoside I inhibits osteoclastogenesis and protects against ovariectomy-induced bone loss. *Front. Pharmacol.* 13, 874952. doi:10.3389/fphar.2022.874952

Mi, N., Cheng, T., Li, H., Yang, P., Mu, X., Wang, X., et al. (2019). Metabolite profiling of traditional Chinese medicine formula Dan Zhi Tablet: an integrated strategy based on UPLC-QTOF/MS combined with multivariate statistical analysis. *J. Pharm. Biomed. Anal.* 164, 70–85. doi:10.1016/j.jpba.2018.10.024

Mu, X., Liu, J., Li, B., Wei, X., Qi, Y., Zhang, B., et al. (2022). A comparative study on chemical characteristics, antioxidant, and hepatoprotective activity from different parts of Schisandrae Chinensis Fructus. *J. Food Process. Preserv.* 46 (11). doi:10.1111/jfpp.16990

Otto, S., Abu-Id, M. H., Fedele, S., Warnke, P. H., Becker, S. T., Kolk, A., et al. (2011). Osteoporosis and bisphosphonates-related osteonecrosis of the jaw: not just a sporadic coincidence-a multi-centre study. *J. Craniomaxillofac. Surg.* 39 (4), 272–277. doi:10.1016/j.jcms.2010.05.009

Park, C. M., Kim, H. M., Kim, D. H., Han, H. J., Noh, H., Jang, J. H., et al. (2016). Ginseno*side re* inhibits osteoclast differentiation in mouse bone marrow-derived macrophages and zebrafish scale model. *Mol. Cells.* 39 (12), 855–861. doi:10.14348/molcells.2016.0111

Putnam, S. E., Scutt, A. M., Bicknell, K., Priestley, C. M., and Williamson, E. M. (2007). Natural products as alternative treatments for metabolic bone disorders and for maintenance of bone health. *Phytother. Res.* 21 (2), 99–112. doi:10.1002/ptr.2030

Ren, S. M., Zhang, Q. Z., Jiang, M., Chen, M. L., Xu, X. J., Wang, D. M., et al. (2022). Systematic characterization of the metabolites of defatted walnut powder extract *in vivo* and screening of the mechanisms against NAFLD by UPLC-Q-Exactive Orbitrap MS combined with network pharmacology. *J. Ethnopharmacol.* 285, 114870. doi:10.1016/j.jep.2021.114870

Si, L., Winzenberg, T. M., Jiang, Q., Chen, M., and Palmer, A. J. (2015). Projection of osteoporosis-related fractures and costs in China: 2010-2050. *Osteoporos. Int.* 26 (7), 1929–1937. doi:10.1007/s00198-015-3093-2

Sinha, K. M., and Zhou, X. (2013). Genetic and molecular control of osterix in skeletal formation. *J. Cell. Biochem.* 114 (5), 975–984. doi:10.1002/jcb.24439

Song, L., Zhou, Y., Qu, L., Wang, D., Diao, X., Zhang, X., et al. (2023). Exploring effects and mechanism of ingredients of herba epimedii on osteogenesis and osteoclastogenesis *in vitro*. *Comb. Chem. and High Throughput Screen* 27, 2824–2837. doi:10.2174/0113862073243559231023065934

Song, M., Jia, F., Cao, Z., Zhang, H., Liu, M., and Gao, L. (2020). Ginsenoside Rg3 attenuates aluminum-induced osteoporosis through regulation of oxidative stress and bone metabolism in rats. *Biol. Trace Elem. Res.* 198 (2), 557–566. doi:10.1007/s12011-020-02089-9

Tao, Y., Huang, S., Yan, J., and Cai, B. (2019). Determination of major components from Radix Achyranthes bidentate using ultra highperformance liquid chromatography with triple quadrupole tandem mass spectrometry and an evaluation of their anti-osteoporosis effect *in vitro*. *J. Sep. Sci.* 42 (13), 2214–2221. doi:10.1002/jssc.201900146

Vasikaran, S., Eastell, R., Bruyere, O., Foldes, A. J., Garnero, P., Griesmacher, A., et al. (2011). Markers of bone turnover for the prediction of fracture risk and monitoring of osteoporosis treatment: a need for international reference standards. *Osteoporos. Int.* 22 (2), 391–420. doi:10.1007/s00198-010-1501-1

Vimalraj, S. (2020). Alkaline phosphatase: structure, expression and its function in bone mineralization. *Gene* 754, 144855. doi:10.1016/j.gene.2020.144855

Wang, T., Wan, D., Shao, L., Dai, J., and Jiang, C. (2015). Notoginsenoside R1 stimulates osteogenic function in primary osteoblasts via estrogen receptor signaling. *Biochem. Biophys. Res. Commun.* 466 (2), 232–239. doi:10.1016/j.bbrc.2015.09.014

Wang, W., Mao, J., Chen, Y., Zuo, J., Chen, L., Li, Y., et al. (2022). Naringin promotes osteogenesis and ameliorates osteoporosis development by targeting JAK2/STAT3 signalling. *Clin. Exp. Pharmacol. Physiol.* 49 (1), 113–121. doi:10.1111/1440-1681.13591

Weinstein, R. S. (2012). Glucocorticoid-induced osteoporosis and osteonecrosis. *Endocrinol. Metab. Clin. North. Am.* 41 (3), 595–611. doi:10.1016/j.ecl.2012.04.004

Xiao, J., Song, N., Lu, T., Pan, Y., Song, J., Chen, G., et al. (2018). Rapid characterization of TCM Qianjinteng by UPLC-QTOF-MS and its application in the evaluation of three species of Stephania. *J. Pharm. Biomed. Anal.* 156, 284–296. doi:10.1016/j.jpba.2018.04.044

Yuan, S., Chen, J., Cao, Y., Zhao, H., Lin, S., Xiong, J., et al. (2024). Investigation of bioactive components and metabolic pathways of Zhen-Wu-tang in rat plasma and renal tissue by UPLC-Q-TOF/MS. *Phytochem. Anal.* doi:10.1002/pca.3455

Zhang, D., Du, J., Yu, M., and Suo, L. (2022). Ginsenoside Rb1 prevents osteoporosis via the AHR/PRELP/NF-κB signaling axis. *Phytomedicine* 104, 154205. doi:10.1016/j.phymed.2022.154205

Zhang, X., Huang, F., Chen, X., Wu, X., and Zhu, J. (2020). Ginsenoside Rg3 attenuates ovariectomy-induced osteoporosis via AMPK/mTOR signaling pathway. *Drug Dev. Res.* 81 (7), 875–884. doi:10.1002/ddr.21705

Zhao, B. J., Wang, J., Song, J., Wang, C. F., Gu, J. F., Yuan, J. R., et al. (2016). Beneficial effects of a flavonoid fraction of herba epimedii on bone metabolism in ovariectomized rats. *Planta Med.* 82 (4), 322–329. doi:10.1055/s-0035-1558294